Polymer 289 (2023) 126477

Contents lists available at ScienceDirect

Polymer

journal homepage: www.elsevier.com/locate/polymer

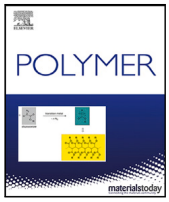

Shear yielding and crazing in dry and wet amorphous PLA at body temperature

Huanming Chen [a], Zhouzhou Pan [a], Daohe Yuan [b], Gregory S. Sulley [b], Reece N. Oosterbeek [a], Charlotte K. Williams [b], Laurence Brassart [a,*]

[a] Department of Engineering Science, University of Oxford, Oxford OX1 3PJ, United Kingdom
[b] Department of Chemistry, University of Oxford, Oxford OX1 3TA, United Kingdom

ARTICLE INFO

Keywords:
Biodegradable polymer
Water-induced plasticisation
Viscoelasticity
Viscoplasticity
Digital image correlation

ABSTRACT

Understanding the inelastic, rate-dependent mechanical response of biodegradable polymers is important for the design of load-bearing biodegradable structures with controlled deformation and failure response. In this study, we investigate the mechanical response of amorphous polylactic acid (PLA) in dry and wet conditions prior to the onset of degradation at body temperature. The presence of water decreases the glass transition temperature by 4.5 °C, the storage modulus by 21%, and the compressive and tensile yield strengths by about 10%, despite a small water uptake of 0.93 wt%. The tensile response of PLA is dominated by craze yielding, rather than shear plasticity, and is stable against necking despite pronounced strain softening and local strain heterogeneities measured by Digital Image Correlation (DIC). Further analysis of the DIC strain fields in dry and wet samples suggests a transition from pure craze yielding in dry samples to a coexistence of craze yielding and shear plasticity in wet samples. The mechanism shift between tension and compression behaviour of dry and wet PLA has implications for the design of load-bearing structures and for constitutive modelling.

1. Introduction

Polylactic acid (PLA) is one of the most promising biodegradable polymers for a broad range of biomedical applications, including orthopaedic fixtures, tissue engineering, drug delivery and cardiovascular stents [1–4]. However, implementation of PLA in load-bearing applications remains challenging, due to the high sensitivity of the mechanical properties on the testing conditions, including water content, temperature and strain rate [5–9], as well as the degradation-induced evolution of the mechanical properties in service. This study focuses on purely amorphous PLA in dry and wet conditions before the onset of degradation at body temperature, with emphasis on the viscoelastic and viscoplastic properties.

Several studies have investigated the large deformation behaviour of PLA. The compression response of purely amorphous PLA was shown to be highly rate dependent, with strong post-yield softening and limited rehardening [10–12]. The rate dependency of the flow stress was shown to be well described by Eyring's equation. While the PLA response in tension at room temperature is generally accepted to be brittle-like, several studies reported significant ductility in tension under various conditions of temperature and water intake [8,13–16]. For example, Stoclet et al. [13] reported a brittle-to-ductile transition in PLA between 25 °C and 35 °C, with ductile deformation at high temperature involving the propagation of a neck through the sample before failure at strain above 200%. These authors further reported simultaneous crazing and shear banding during plastic deformation. Rezgui et al. [14] also reported high ductility (about 150%) in their PLA at 50 °C accompanied by significant volume change attributed to cavitation. Sweeney et al. [17] carried out biaxial stretching and relaxation experiments on PLA at 60 °C, also achieving large extension ratios and showing strong post-yield softening. Other studies reported that PLA at room temperature had much reduced post-yield softening and ductility of the order of 10% strain [18,19]. Constitutive models have also been developed to simulate the rate-dependent response and post-yield softening in tension [16,17,19], however these models did not attempt to distinguish shear plasticity from craze yielding in their phenomenological description. The plasticising effect of water on the physical properties of polymers is also well known [20,21]. The blending of small molecules with long polymer chains increases the chain mobility [22–24]. Water molecules can also break intermolecular bonds, further leading to increased chain mobility [20,21,25]. The increase in chain mobility in turn leads to a decrease in the glass transition temperature [22,26,27], and a reduction in elastic modulus and yield stress [8,22,27].

* Corresponding author.
E-mail address: laurence.brassart@eng.ox.ac.uk (L. Brassart).

https://doi.org/10.1016/j.polymer.2023.126477
Received 14 September 2023; Received in revised form 7 November 2023; Accepted 8 November 2023
Available online 10 November 2023

In this study, we conducted an extensive mechanical characterisation campaign on an industrial PLA grade, Natureworks 4060D, in both dry and wet conditions at 37 °C. This grade possesses a stable amorphous structure with very little tendency to crystallise. Amorphous PLA was selected as a model material to study the interplay between hydration, degradation and mechanical properties, without the added complexity brought about by a semi-crystalline microstructure. Thermo-mechanical characterisation included Differential Scanning Calorimetry (DSC) and Dynamic Mechanical Analysis (DMA), as well as conventional quasi-static uniaxial tension and compression tests at various strain rates, coupled with Digital Image Correlation (DIC) analysis of the surface strain field. Our results suggest that the tensile behaviour of dry amorphous PLA at body temperature is dominated by craze-yielding, rather than shear plasticity. Crazing remains significant in accommodating the tensile deformation in wet amorphous PLA, however we hypothesise that shear plasticity and crazing coexist in wet conditions at body temperature. Our findings have implications for the development of constitutive models for these materials, which should properly account for the different deformation mechanisms in tension and compression and the presence of water. The distinct deformation mechanisms in tension and compression are also likely to impact structural performance during degradation.

2. Experimental methods

2.1. Material and sample preparation

The PLA used in this study is the Ingeo™4060D grade from NatureWorks LLC [28], which is supplied in pellet form. This is an amorphous polymer with about 12% D-lactide isomer content [29]. The glass transition temperature of this polymer is in the range 50–60 °C and the melting temperature is in the range 150–180 °C [28]. The distribution of molecular weight was characterised with a Shimadzu high-performance liquid chromatography (HPLC) system, using tetrahydrofuran (THF) as eluent. The number- and weight-average molecular weights of the as-received pellets were 129 kg/mol and 195 kg/mol, respectively.

Injection moulding is commonly used to process PLA, however it is also known to produce inhomogeneous microstructures and residual stresses in the final product [30–33]. In this study, an alternative melt-to-mould method was used to reduce chain stretching and alignment during processing. Neat pellets were moulded into 7-mm thickness flat sheets at 180 °C under a 2-cm thick PTFE sheet which produced a pressure of 0.4 kPa, then naturally cooled to room temperature (Fig. S1). The number- and weight-average molecular weights measured by HPLC after moulding decreased to 103 ± 4 kg/mol and 175 ± 8 kg/mol, respectively, which is attributed to the possible hydrolytic degradation in the presence of residual water. The density of PLA sheets was 1.24 g/cm^3, consistent with the data sheet. DSC scans before and after processing (Fig. S2) confirm that the polymer remains fully amorphous after moulding. This is consistent with literature reports that PLA with D-isomer content above 8% cannot crystallise [34,35]. D-isomers bring about stereoregularity defects, disturbing the chain arranging mechanism and limiting the formation of cohesive structure (mesophase) and crystallites. Chains are also more likely to relax any processing-induced orientation or stretching [35]. Note however that partial crystallisation in this PLA grade is possible during hydrolytic degradation [29,36], however this effect is negligible in the present study, as verified below.

The PLA sheets were polished on both sides to the desired thickness using a fly cutter, and then machined into various specimen shapes: cylindrical specimens for compression testing (height: 4 mm, diameter: 5 mm), dog-bone shape specimens for tensile testing (ISO527 type 1BA with a 2-mm thickness and 25-mm gauge length), and beam-shape specimens for DMA testing (36 mm × 8 mm × 2 mm). Cutting speeds were carefully controlled to prevent overheating and melting of the plate surface (700 rpm for surface polishing, and 400 rpm for CNC routing and turning). A compressed air jet was mounted on the tool tip to effectively dissipate the heat generated in the cutting process zone. Plates and machined specimens were carefully examined using an in-house polariscope (Fig. S3) following ASTM D4093-95, showing no apparent defects or flow lines. No differences in the mechanical properties of tested specimens cut from the sheets in random orientations were observed, suggesting in-plane isotropy of the material.

To alleviate the effect of different thermal histories in the bulk and on the surface of the material, all specimens were annealed before testing at 50 °C (below T_g) for 6 h and naturally cooled to room temperature at about 0.12 °C/min on average. Annealed specimens were then conditioned at room temperature for approximately a half day before testing. No significant differences were observed in the stress–strain responses of specimens tested within a few hours time interval.

Hydrated samples were prepared by immersing specimens in phosphate buffered saline (PBS) solution (Sigma Aldrich, UK) with pH 7.4 at 37 °C for up to three weeks. The ratio of PBS volume to specimen mass was set to 60 ml/g, twice the minimum ratio recommended by the ISO-15814 standard. Specimens were individually sealed in PBS-containing glass vessels, and glass vessels were immersed in a water-containing petri dish maintained at 37 °C by a 30 W silicone heater mat (RS, UK). The PBS solution inside the glass vessels was refreshed every 24 h using a syringe, and the pH was measured daily using a benchtop pH-meter (Fisherbrand, UK). The decrease in the solution pH over one day was less than 0.04. Specimen weights were measured before immersion (M_i), just after immersion for a set amount of time (M_w), and after subsequent drying at 50 °C for 5 days (M_d). The water uptake W was calculated from $(M_w - M_d)/M_d$, and the weight loss was calculated from $(M_i - M_d)/M_i$. At least three specimens were tested for each measurement point to ensure reproducibility.

2.2. Thermo-mechanical characterisation

Thermal properties of dry and wet PLA were examined by Differential Scanning Calorimetry (DSC) using a TA DSC Q2000. Test specimens (about 3.5 mg) were extracted from the centre of hydrated beam-shape specimens, sealed into aluminium pans, and subjected to heating and cooling cycles from −20 °C to 180° at a constant rate of 5 °C/min. The glass transition temperature (T_g) was determined from the heat flow as the midpoint temperature of heat flow inflection according to ASTM E1356-08.

The small-strain thermo-mechanical properties were characterised by Dynamic Mechanical Analysis (DMA) using a TA Instruments Q800. Beam-shape specimens were tested in single-cantilever configuration (gauge length: 17.50 mm) and subjected to temperature sweeps at frequencies $f = 0.1$, 0.5, 1, 3 and 10 Hz. Temperature sweeps were performed at 2 °C intervals from −60 °C to 76 °C on the dry specimens, and from 2 °C to 76 °C on hydrated specimens. The strain amplitude ϵ_0 was set to 0.1%. The storage modulus E', loss modulus E', and loss tangent $\tan\delta = E''/E'$ were measured.

2.3. Mechanical testing and DIC

Quasi-static uniaxial tension and compression tests were performed using a commercial screw-driven load frame (Instron 5980) with a 10 kN load cell equipped with an environmental chamber (Instron 3119) at a constant temperature of 37 °C. Compression tests were performed on cylindrical specimens at constant true strain rates of 0.001, 0.01, and 0.1 s^{-1}. The inelastic compression response of glassy polymers is dominated by shear plasticity, which is essentially volume preserving [37]. Therefore, the true stress in the loading direction x_3 was estimated based on the assumption that the volume remains constant during deformation as: $\sigma_3 = F/A = (F/A_0)(H/H_0)$, where F is the force, H_0 and H are the specimen initial and deformed heights, and A_0 and A are the specimen initial and deformed areas. Note that we have also neglected the volume change due to elastic deformations

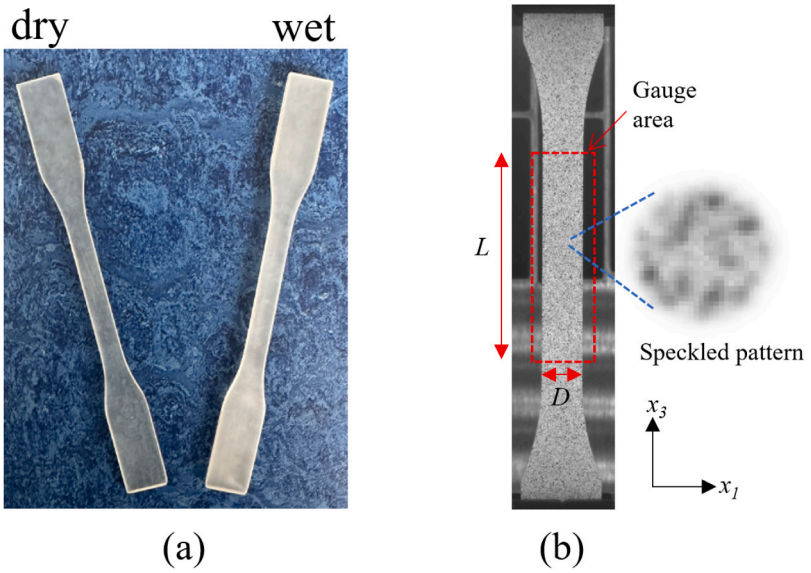

Fig. 1. (a) Dog bone-shaped tensile specimens in dry and hydrated conditions after 6 days of immersion in PBS. (b) Speckled pattern on the surface of a tensile specimen. Total true strains were obtained from DIC measurements of the deformed length and width of the gauge area.

(the Poisson's ratio of PLA is 0.35). This approximation is acceptable provided that the extent of plastic deformation is much larger than the extent of elastic deformation.

Tensile tests were conducted on dog-bone specimens (Fig. 1(a)) at constant cross-head velocity, $V_{\text{c-h}}$ of 0.03, 0.3 and 3 mm s^{-1}. Specimens were spray painted (Fig. 1(b)) and DIC analysis of the displacement and strain fields was performed using the commercial software MatchID [37]. The equipment and DIC parameters are listed in Table S1. The local volume change was calculated from the transverse and longitudinal strains, ε_1 and ε_3, as:

$$\varepsilon_v = 2\varepsilon_1 + \varepsilon_3, \tag{1}$$

where we assumed isotropic deformation in the plane transverse to the tension direction: $\varepsilon_1 = \varepsilon_2$. In addition to measuring the local strain fields, we also used DIC as a multiaxial extensometer to measure the total change in length and width of the gauge region. The corresponding total true strains for the gauge region were calculated as: $\bar{\varepsilon}_3 = \ln(L/L_0)$ and $\bar{\varepsilon}_1 = \ln(D/D_0)$ where L and L_0 are the deformed and initial gauge lengths, and D and D_0 are the deformed and initial gauge widths. The total volume change was then calculated as: $\bar{\varepsilon}_v = 2\bar{\varepsilon}_1 + \bar{\varepsilon}_3$. Here we used the word 'total' to distinguish the strain calculated based on the overall dimensions of the gauge region from the local strain measurements based on individual marker displacements within the gauge region. In the following, we omit the overbar notation for simplicity when it is clear from the context that overall measures for the whole gauge region are used. Note that the total true strain rate calculated from DIC measurements is not constant. Finally, the true stress in the tensile direction was calculated as: $\sigma_3 = F/A = (F/A_0)\exp(-2\bar{\varepsilon}_1)$.

Optical microscopy was used to observe the development of crazes during tensile deformation. A tensile specimen was abraded with sand paper to expose the sub-surface and to remove surface scratches, and subjected to interrupted tensile loading at a 0.03 mm s^{-1} cross-head velocity. The sample surface was examined with an Olympus BX51TRF microscope, using a polarising filter to reduce surface reflections and increase the image contrast. Both dry and wet specimens were examined, however only dry (transparent) specimen results are presented here, which gave the best quality of micrograph contrast.

3. Hydration experiments

Hydration experiments were conducted to identify a suitable immersion period, such that the PLA samples are fully saturated in water but the effect of hydrolytic degradation on the thermo-mechanical properties can be assumed negligible. The time evolution of water uptake in specimens with cylindrical, dog-bone and beam shape is shown in Fig. 2(a), showing similar trends for all specimen shapes. Water uptake is fast in the first few days of immersion, reaching 0.93 wt% on average after 6 days, followed by a much slower water absorption response reaching 1.05 wt% on average after 20 days. The diffusion coefficient of PLA was estimated by fitting experimental data for the beam-shape specimens using the classical solution for Fickian diffusion through a plane sheet [38]:

$$\frac{W(t)}{W_\infty} = 1 - \sum_{n=0}^{\infty} \frac{8}{(2n+1)^2\pi^2} \exp\left\{-D(2n+1)^2\pi^2 t/4l^2\right\}, \tag{2}$$

where $W(t)$ represents the water uptake at time t (in wt%), and W_∞ represents the water uptake at saturation. D is the (assumed constant) diffusion coefficient of water in PLA, and l is the half-plane thickness. The saturation water uptake was set equal to the water uptake after 6 days: $W_\infty = 0.93$ wt%, and D was fitted on the experimental data via Eq. (2), giving $D = 4 \times 10^{-8}$ cm^2 s^{-1}. This is comparable to the diffusivity coefficient $D = 6.4 \times 10^{-8}$ cm^2 s^{-1} at 37 °C reported by Lyu et al. [39]. The fitted curve is represented as a dashed line in Fig. 2(a). The 1D model very well captures the water uptake response in beam-shape specimens. Faster water uptake in dogbone-shape and cylindrical specimens is attributed to a non-negligible water ingress from other surfaces, so that Eq. (2) is less valid.

In contrast to the prediction of the Fickian diffusion model (2), water uptake does not fully saturate in the experiments. This is could be due to hydrolysis, which increases water solubility in the polymer [40]. Fig. 2(b) shows the evolution of the molecular weight during immersion in water. The full molecular weight distributions are shown in Fig. S4. The average molecular weight remained approximately constant for the first 6 days of immersion, after which it started to decrease slowly. The weight loss after 21 days was about 0.06 wt%. These observations suggest that PLA samples immersed in water at 37 °C for 6 days can

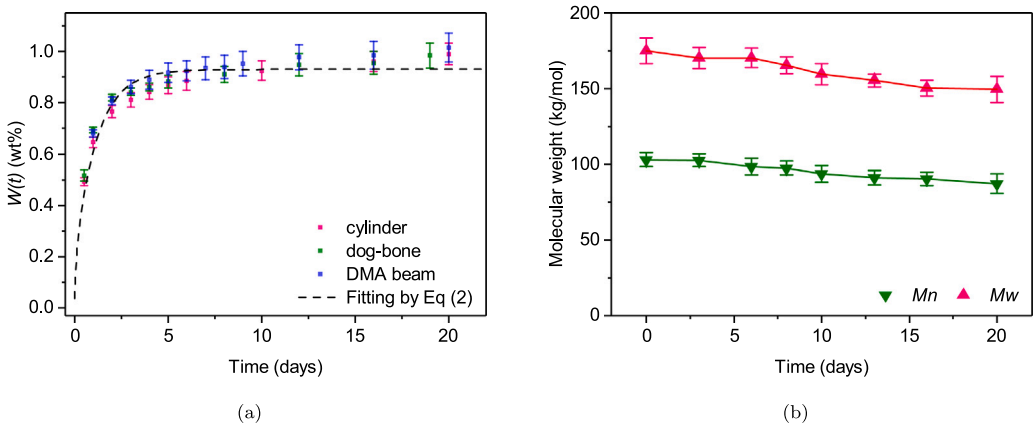

Fig. 2. (a) Water uptake during immersion in 37 °C PBS as a function of time in cylindrical, dog-bone and beam-shape specimens. The dashed line is the fitting of the experimental curve for the beam-shape specimen using Eq. (2), with $D = 4 \times 10^{-8}$ cm^2 s^{-1} and $W_\infty = 0.93$ wt%. (b) Average molecular weight as a function of immersion time.

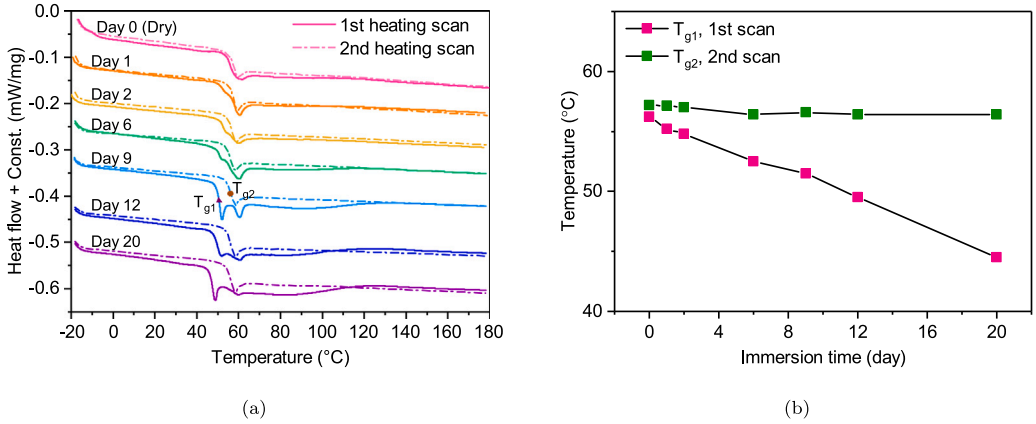

Fig. 3. (a) Heat flow profiles measured by DSC for PLA specimens after different immersion periods. An arbitrary constant was added to the heat flow to distinguish curves for different specimens. (b) Glass transition temperature identified from each heat scan curve.

be considered as fully saturated and with negligible hydrolysis. In the following, we use the term 'wet PLA' to refer to material samples immersed in water at 37 °C for 6 days, unless otherwise indicated.

4. Thermo-mechanical characterisation results

4.1. DSC

DSC thermograms of dry and wet PLA specimens after different immersion periods up to 20 days are shown in Fig. 3(a). No melting peaks were detected, indicating that the polymer remained amorphous, as expected. For the dry PLA, heat flow curves were almost identical during the first and second heating scans. In contrast, wet samples displayed different heat flow curves during the first and second heating scans, with the first heating curves varying with the immersion period, and the second heating curves similar to that of the dry samples. The glass transition temperatures T_{g1} and T_{g2} calculated from the first and second heating scans are shown in Fig. 3(b) as function of the immersion time. T_{g1} decreased significantly with the immersion time, dropping from the initial value of 56 °C for dry samples down to 44 °C after 20 days of immersion, while T_{g2} displayed only a small decrease from 57 °C to 56.4 °C over the same time period. The difference between the T_{g1} of dry samples and that of wet samples immersed in water for 6 days was 4.1 °C.

The similarity of the second heating curves, independent of the immersion period, can be explained by the evaporation of water which happens during the first heating scan (see below). At the end of the first scan, all samples consist of molten polymer with no residual water, so that subsequent cooling and re-heating at constant rate produces near-identical heat curves and hence similar T_g values. The small drop in T_{g2} after a few days of immersion can be correlated to the slight drop in molecular weight (Fig. 2(b)) over the same immersion period. Interestingly, the enthalpy relaxation peak resulting from cooling between the two heat scans is the same as the enthalpy relaxation peak observed in dry samples.

The difference between the first and second heating curves in wet samples is attributed to the presence of water. The decrease in glass transition temperature T_{g1} is a manifestation of the plasticising effect of water, which increases the segmental mobility of the chains and triggers primary structural relaxation at lower temperature [20]. Glass transition in wet samples is immediately followed by a narrow endothermic overshoot, which increases as the immersion time increases. Similar features in DSC curves of PLA were reported in [27]. This overshoot is associated with partial evaporation of water [41]. A secondary endothermic peak is also seen during the first heating scan of wet samples, which is attributed to enthalpy relaxation. Following the endothermic peaks in the glass transition region, a gap between the first and second heat curves persists until about 100 °C, and the gap increases with the immersion time. This gap is associated with the presence of residual bound water, which evaporates at the water boiling point or above [42].

Fig. 2(b) shows that T_{g1} decreases almost linearly with immersion time over a 20 days period, although absorbed water reaches near-saturation after about 6 days. Thus, the plasticising effect of water is not proportional to the water content. Hydrolysis is unlikely to be the reason for the continued decrease in T_{g1} after water saturation, since

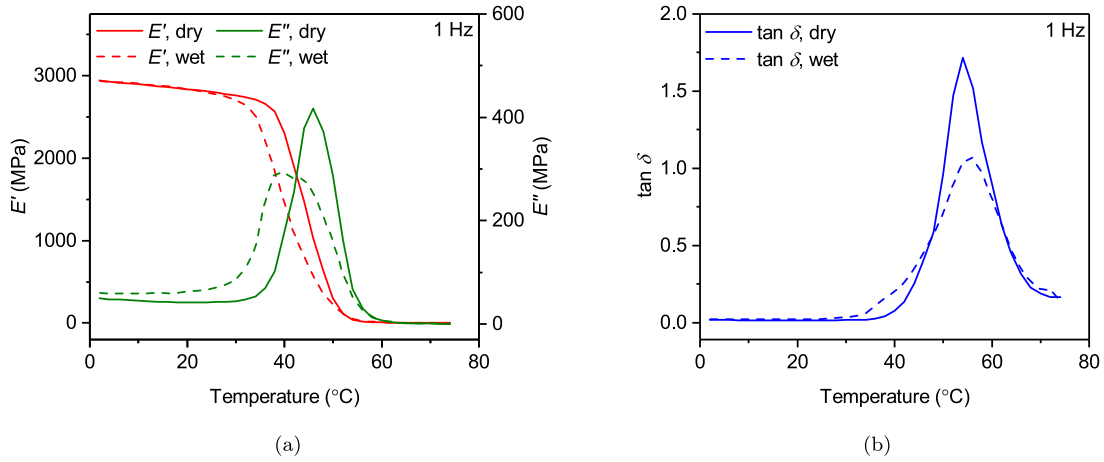

Fig. 4. DMA measurements of (a) storage modulus (E'), loss modulus (E''), and loss tangent $\tan\delta = E''/E'$ for dry and wet PLA in temperature sweeps at loading frequency $f = 1$ Hz and strain amplitude $\epsilon_0 = 0.001$.

T_{g2} is largely independent of the immersion period, in contrast with the expected hydrolysis-induced shift of T_g [29,43]. We hypothesise that the decrease in T_{g1} in water-saturated PLA results from molecular rearrangements with a kinetics distinct from the water sorption kinetics. Such rearrangements might include the breaking of interpolymer H-bonds by water, which would lead to increased molecular mobility, and hence to further reduction in T_g [20]. More advanced characterisation techniques would be required to elucidate this point, e.g. [25,44].

4.2. DMA

The storage and loss moduli of dry PLA and that of wet PLA immersed in PBS for 6 days were measured over a 2–76 °C range at frequencies $f = 0.1, 0.5, 1, 3$ and 10 Hz. Representative data for E' and E'' at $f = 1$ Hz are shown in Fig. 4(a), and the corresponding loss tangent $\tan\delta = E''/E'$ is shown in Fig. 4(b). Data for all frequencies are shown in Fig. S5. Dry specimens have a higher storage modulus than wet specimens at the same temperature and frequency. At 1 Hz and 37 °C, the drop in storage modulus induced by the presence of water is 21%. The glass transition temperature T_g at each loading frequency was estimated in three different ways: (i) from the point of largest slope in E', (ii) the E'' peak, and (iii) the loss tangent peak, and are reported in Table S2. Regardless of the method used, the T_g value of wet samples was always lower than that of dry samples.

The frequency dependence of T_g is illustrated in Fig. 5, where T_g was measured from the drop in E', suggesting a linear dependence of T_g on $\log f$ with a similar slope for both dry and wet samples. The difference between the glass transition temperature of dry and wet PLA at a given frequency (vertical shift) was 4.5 °C, approximately independent of frequency in this frequency range. The reduction in T_g measured from DMA is similar to the drop in T_{g1} measured by DSC (4.1 °C).

The Time-Temperature Superposition (TTS) principle was used to estimate the rheological properties of dry and wet PLA over a broad range of frequencies from the temperature sweep data. For each temperature, data for E' were first plotted as a function of $\log f$, and then manually shifted to produce a smooth master curve at the reference temperature $T_{\text{ref}} = 37$ °C. Master curves for dry and wet PLA are shown in Fig. 6(a). The storage modulus of dry samples at 37 °C is higher than that of wet samples across the glass transition region, but is the same as that of wet samples at both low and high frequencies. In Fig. 6(a), the dashed lines represent the fitting of the discrete master curves using the Generalised Maxwell Model (GMM). Parameters of the GMM are provided in Table S3. The validity of the TTS principle was also verified taking either $T_{\text{ref}} = T_{\text{g,dry}} = 46$ °C (Fig. S6) or $T_{\text{ref}} = T_{\text{g,wet}} = 41.5$ °C (Fig. S7), where $T_{\text{g,dry}}$ and $T_{\text{g,wet}}$ are the glass transition temperatures

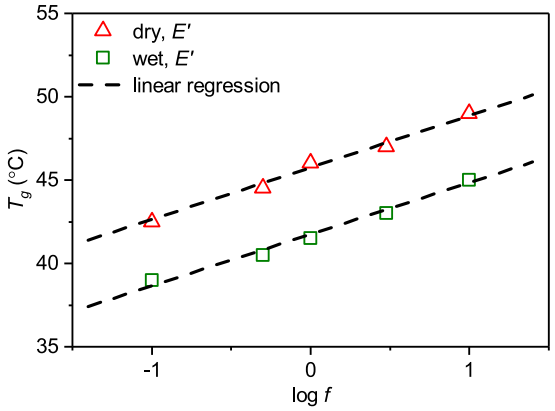

Fig. 5. Dependence of T_g (measured from the drop in E') on the loading frequency for day and wet PLA. The dashed line represents a linear regression with slope 3.1 °C per decade.

of the dry and wet PLA at the reference frequency $f = 1$ Hz measured from the drop in E' (Table S2).

Interestingly, the shift factors $\log a_T(T)$ used to produce the master curves of dry and wet PLA are almost identical (Fig. 6(b)), except in the high and low temperature regions. The dependence of the shift factor on temperature in the glass transition region is well described by the Williams–Landel–Ferry (WLF) equation:

$$\log a_T = -\frac{C_1\left(T - T_{\text{ref}}\right)}{C_2 + \left(T - T_{\text{ref}}\right)}, \tag{3}$$

where C_1, C_2 are fitting parameters. For $T_{\text{ref}} = 37$ °C, these were identified as $C_1 = 22.8$ and $C_2 = 50.1$. For $T_{\text{ref}} = T_{\text{g,dry}}$ or $T_{\text{ref}} = T_{\text{g,wet}}$, a good fit was obtained using the universal values identified by Williams, Landel and Ferry: $C_1 = 17.44$ and $C_2 = 51.6$ [45] (Figs S3(b) and S4(b)). For temperatures below the glass transition temperature, the relationship between the shift factor and the temperature can be described Arrhenius equation, see e.g. [46]:

$$\log a_T = -\frac{E_a}{2.303R}\left(\frac{1}{T} - \frac{1}{T_{\text{ref}}}\right), \tag{4}$$

where E_a is the activation energy and $R = 8.3145$ J K^{-1} mol^{-1} is the gas constant. For $T_{\text{ref}} = 37$ °C, the fitted activation energy was found as $E_a = 4.5 \times 10^5$ J mol^{-1}, the same for dry and wet PLA.

Eq. (3) can be used to relate the shift in T_g with the loading frequency. By differentiating Eq. (3) with respect to T, and taking the

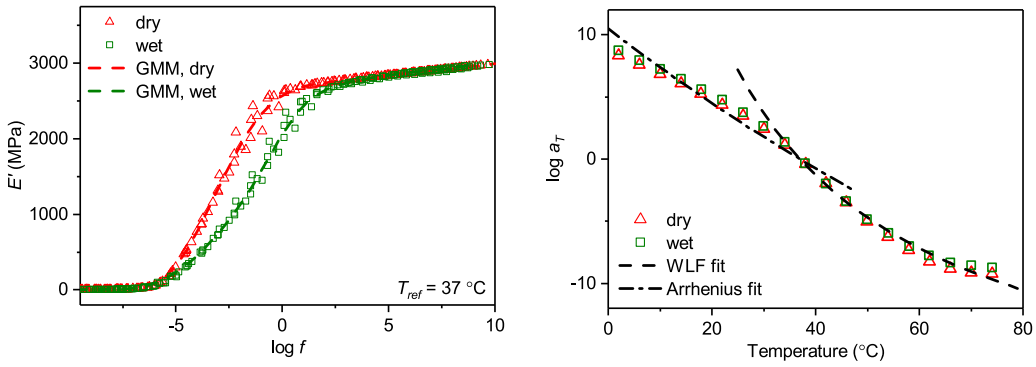

(a) (b)

Fig. 6. (a) Application of TTS to dry and wet PLA with T_{ref} = 37 °C. Dashed line represent the fitting of the discrete master curves using the generalised Maxwell model. (b) Shift factors for dry and wet PLA used to construct the discrete master curves, and partial fits using Arrhenius and WLF equations.

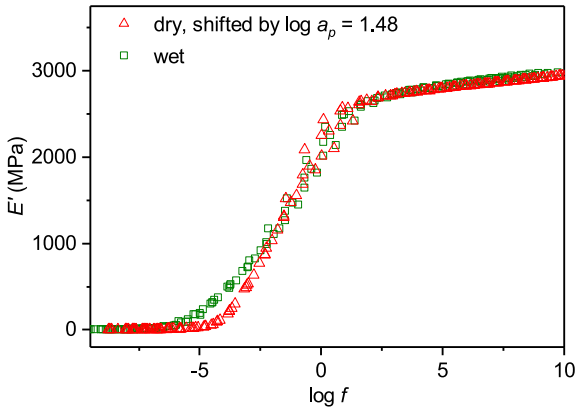

Fig. 7. Shifted master curve of PLA towards the master curve of wet PLA, obtained using a shift factor $\log a_P = 1.48$ to the right, corresponding to a increase in temperature $\Delta T = 4.5$ °C.

limit $T \to T_{\text{ref}}$, we obtain [47]:

$$\frac{d \log f}{dT} = \frac{C_1}{C_2}. \tag{5}$$

Using the universal values of the WLF constants which hold for $T_{\text{ref}} = T_g$, we find $\frac{dT}{d \log f} = 2.96$ °C in the vicinity of T_g. This value is consistent with the slope of 3.1 °C per decade of the linear regressions in Fig. 5.

The softer response of wet PLA compared to that of dry PLA at a given loading frequency is attributed to the plasticisation effect of water. To investigate a possible equivalence between the presence of water and a change in loading frequency, Fig. 7 shows the modified master curves for dry and wet PLA, where the master curve for dry PLA (Fig. 6(a)) has been shifted to the right by a constant shift factor $\log a_P = 1.48$, equal to the horizontal shift between raw data for dry and wet PLA at 37 °C (where $\log a_T = 0$). The agreement is good, except in the low frequency region where the shift factors for dry and wet PLA deviate (Fig. 6(b)). As a result, it is not possible to collapse the master curves for dry and wet PLA using a single plasticising shift factor $\log a_P$ valid at all frequencies, or temperatures. According to the relationship between the shift factor and temperature (Fig. 6(b)), the frequency shift $\log a_P = 1.48$ corresponds to an increase in temperature of $\Delta T = 4.5$ °C. This is the same temperature difference as the difference between the glass transition temperatures $T_{\text{g,dry}}$ and $T_{\text{g,wet}}$.

Previous studies have shown that time-water superposition principle applies to many polymers, according to which curves for E' as a function of $\log f$ measured for various water contents collapse onto a single master curve at a reference water content [48–52]. In this work, we did not characterise the rheological properties of wet PLA at various water contents, so that the validity of a time-water superposition principle for wet PLA could not be fully investigated.

5. Plastic behaviour in tension and compression

5.1. Compression behaviour

Representative true stress–strain curves for dry and wet PLA (6 days of immersion) in compression are shown in Fig. 8 (all repeats are shown in Fig. S8). Here we used the notation: $\varepsilon = |\varepsilon_3|$ and $\sigma = |\sigma_3|$. All curves exhibit pronounced post-yield softening with average stress drop of 52%, followed by a plateau and rehardening at large deformation. The yield stress (defined as the maximum stress) increases with the strain rate and is lower in wet samples for the same loading rate by about 11% on average.

Interestingly, the post-yield flow stress in samples tested at rate $\dot{\varepsilon} = 0.1$ s^{-1} becomes smaller than that of samples tested at $\dot{\varepsilon} = 0.01$ s^{-1} at compression strains larger than about 0.2 for dry samples, and 0.4 for wet samples. We attribute this effect to adiabatic heating [53,54], based on the following analysis. Let l be the characteristic size of the specimen, and α be the thermal diffusivity of the material, defined as $\alpha = K/\rho C_p$, with K the thermal conductivity, ρ the mass density and C_p the specific heat. The thermal diffusivity and the characteristic size of the specimen together define a characteristic time for heat to diffuse out of the specimen: $\tau = l^2/\alpha$. Adiabatic heating requires that the characteristic time scale for the experiment, τ_{exp}, be much smaller than τ:

$$\tau_{exp} \ll \frac{l^2}{\alpha}. \tag{6}$$

For dry PLA, $K = 0.08$ (J s^{-1} m^{-1} K^{-1}) [55], $\rho = 1240$ kg m^{-3}, and $C_p = 1420$ J kg^{-1} K^{-1} (as measured by DSC). For specimens with a characteristic length $l = 2$ mm, the characteristic time for thermal diffusion is thus of the order of 88 s. Experimental time scales for the compression experiments carried out at $\dot{\varepsilon} = 0.001$, 0.01 and 0.1 s^{-1} up to a strain $\varepsilon_f = 0.8$ have time scales of 800 s, 80 s and 8 s, respectively. The above calculation thus predicts that testing at a strain rate of 0.1 s^{-1} can cause adiabatic heating. We next estimated the temperature increase caused by adiabatic heating from the relation:

$$\Delta T = \frac{\beta}{\rho C_p} \int_{\varepsilon_y}^{\varepsilon_f} \sigma(\varepsilon)\, d\varepsilon, \tag{7}$$

where β is the Taylor-Quinney coefficient giving the plastic work to heat conversion factor (set to 1 here for simplicity), and ε_y is the yield strain [56]. Using the experimental stress–strain curve at $\dot{\varepsilon} = 0.1$ s^{-1}, Eq. (7) gives an estimated temperature increase of up to 18 °C (Fig. S9), which would be sufficient to cause material softening at large deformation. This value should however be taken as an upper bound, since we

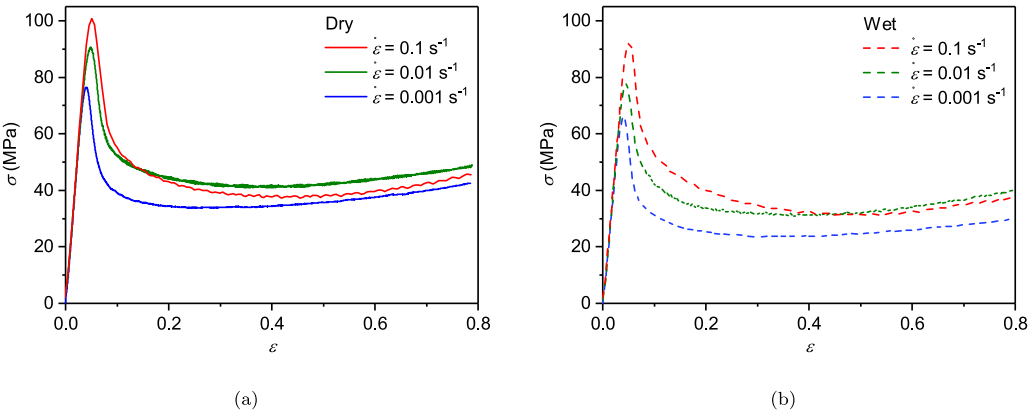

Fig. 8. True stress–strain compression response for (a) dry and (b) wet specimens.

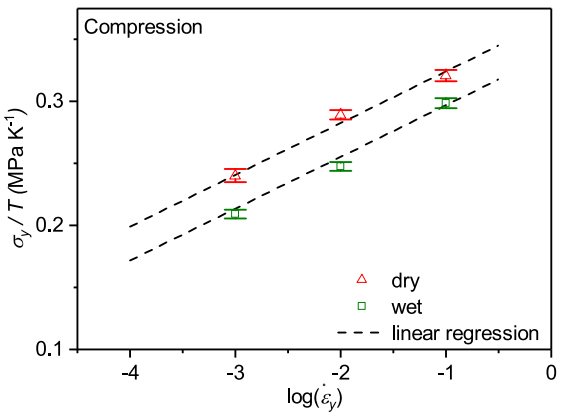

Fig. 9. Strain-rate dependence of the yield stress and linear regressions with a slope of 0.042 MPa K^{-1} per decade for both dry and wet specimens.

used $\beta = 1$. The reduced adiabatic effect in wet samples is attributed to the larger heat capacity of water, compared to that of dry PLA.

The strain rate dependence of the yield stress is illustrated in Fig. 9, showing a linear dependence of the yield stress on the logarithm of the strain rate with a slope of 0.042 MPa K^{-1} per decade, the same for both dry and wet specimens. This value is similar to the slope calculated based on data from the literature for various PLA grades [10,11,57,58], see Section S5.

5.2. Tension behaviour

Representative stress–strain curves for the tensile response of dry and wet PLA after 6 days of immersion are shown in Fig. 10 (all the repeats are shown in Fig. S11). As explained in Section 2.3, tensile tests were conducted at constant cross-head velocity, and the total true strain, shown in the figures, was calculated by DIC. The yield stress increases and the elongation at break decreases as the strain rate increases. Curves show post-yield softening of about 8%, much less pronounced than in the compression case. The tensile yield stress of wet samples is lower than that of dry samples by about 10% on average. PLA exhibits only modest ductility in tension, and samples failed in a brittle manner without showing any necking, suggesting a craze-yielding mechanism, rather than shear plasticity.

The rate dependence of the yield stress is shown in Fig. 11. Given that the true strain rate is not constant in tensile tests performed at constant cross-head velocity, here the yield stress (divided by the absolute temperature) is plotted as a function of the true strain rate measured by DIC at the yield point. Dashed lines in the figure correspond to a linear regression with a slope of 0.025 MPa K^{-1} per decade, the same for dry and wet samples. The fracture strain at the different cross-head velocities is shown in Fig. 12. The fracture strain appears larger in wet samples, while no clear trend emerges from measurements at the highest rate. It is however difficult to draw definitive conclusions regarding the effect of water on the fracture strain, given the large standard deviation.

Fig. 13 shows the development of intense crazing on the specimen surface at different levels of applied strain. At a small strain below the yield strain (a), a large number of very thin crazes are observed with average length of about 100 μm. As the strain approaches the yield strain (b), crazes grow rapidly to reach a length of about 250 μm, without much change in width. Past the yield strain (c), crazes broaden and possibly merge. As the strain increases further (d)–(e), crazes further widen from 20 μm to 80 μm until final failure.

Craze-dominated plastic deformation in tension is confirmed by the very large volume change during deformation. Fig. 14 shows the evolution of the total longitudinal and transverse strains measured by DIC as a function of time for dry and wet specimens tested at a cross-head velocity of 0.03 mm s^{-1}, and the corresponding volumetric strain. In the elastic deformation regime, the rate of lateral contraction during tensile testing corresponds to Poisson's ratio ($\nu = 0.35$). However, after the yield point, the ratio of transverse strain rate to longitudinal strain rate decreases sharply (Fig. 14(a),(c)), and the volume change increases steeply (Fig. 14(b),(d)). In dry specimens, the volume change accumulated during plastic deformation is almost identical to the longitudinal strain, i.e. there is almost no transverse contraction. In wet specimens, the accumulated volume change accounts for about two thirds of the longitudinal strain. The same ratios of volumetric to longitudinal strains were found in tensile tests conducted at 0.3 mm s^{-1} (Fig. S13) (specimens tested at 3 mm s^{-1} failed before they could develop significant plastic strain).

Tensile specimens did not show necking during plastic deformation despite the significant strain softening. However, inspection of the full DIC strain fields in the gauge region reveals significant strain heterogeneities. Fig. 15(a),(b) show the fields of longitudinal and volumetric strains in a wet specimen loaded at a cross-head velocity of 0.03 mm s^{-1} at different total longitudinal strains. Strain heterogeneities develop in the post-yield regime ($\bar{\varepsilon}_3 > 0.02$). Heterogeneities in longitudinal strain develop into horizontal bands, while heterogeneities in the volumetric strain are less defined. Significant volume change is seen everywhere in the gauge region. Fig. 15(c),(d) show the corresponding averages of these fields across the width of the gauge region as a function of the vertical distance from the centre of the gauge region, for different total strains. These plots show that significant heterogeneities develop at the yield point, and that their relative amplitudes do not change appreciably during loading. A similar evolution of heterogeneities was observed at a cross-head velocity of 0.3 mm s^{-1}, see Fig. S14.

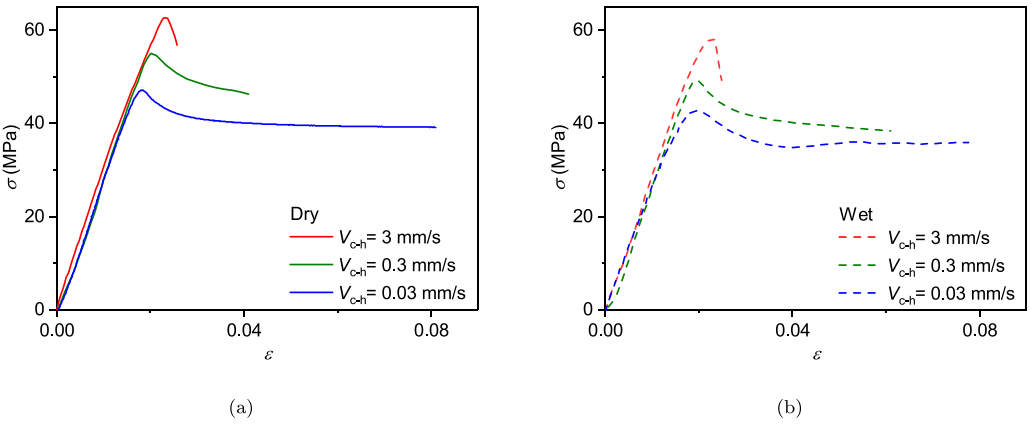

Fig. 10. True stress–strain tensile response for (a) dry and (b) wet specimens tested at different cross-head velocities V_{c-h}.

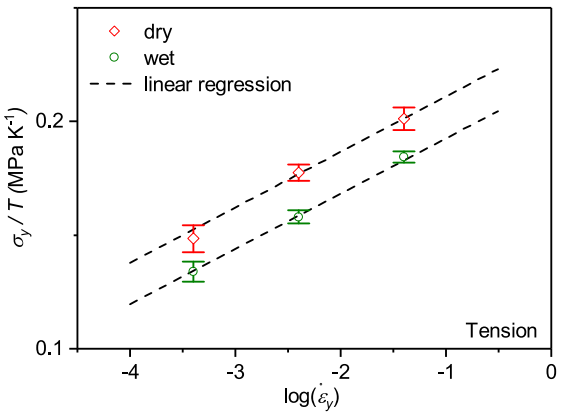

Fig. 11. Strain-rate dependence of the yield stress and linear regressions.

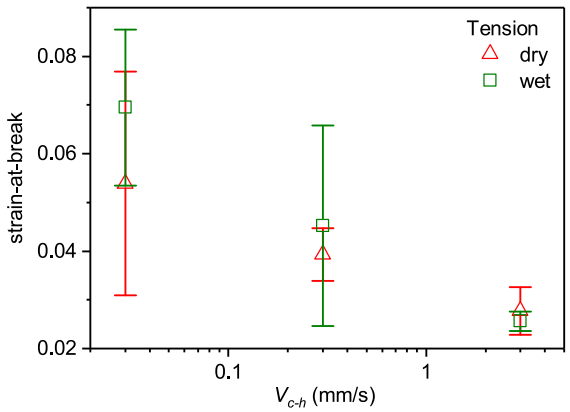

Fig. 12. Strain-to-break in tensile experiments at different cross-head velocities.

Strain heterogeneities are more pronounced in the wet specimen, and the localisation of the longitudinal strain into horizontal bands is less clear (Fig. 16(a),(b)). Different from the dry specimen, some regions show very little volume change up to the point of failure. Width-averaged profiles of the longitudinal and volume strains (Fig. 16(c),(d)) highlight the larger amplitude of the strain heterogeneities, which can exceed the average strain by a large amount. The relative amplitudes of strain heterogeneities also increases during deformation, i.e. the strain heterogeneities are amplified during deformation. Corresponding DIC results for a cross-head velocity of 0.3 mm s^{-1} are shown in Fig. S15.

6. Discussion

6.1. Compression behaviour

The behaviour of PLA in compression (Fig. 8) shows the typical features of shear plasticity in glassy polymers, including pronounced post-yield softening and strong rate sensitivity. Shear plasticity in glassy polymers is mediated by localised thermally-activated molecular rearrangements, called shear transformation zones, facilitated by an applied shear stress [47]. The rate dependency of the apparent yield stress (Fig. 9) is well described by Eyring's equation:

$$\dot{\varepsilon} = \dot{\varepsilon}_0 \exp\left(-\frac{\Delta H}{RT}\right) \exp\left(\frac{\sigma_y V^*}{2RT}\right), \tag{8}$$

where ΔH is the molar activation enthalpy, V^* is the molar activation volume, and $\dot{\varepsilon}_0$ is a reference strain rate. In writing Eq. (8), we have neglected the possible contribution of the hydrostatic pressure to the flow stress. The activation volume for shear transformation is identified from the slope of the linear regressions shown in Fig. 9:

$$\frac{d(\sigma_y/T)}{d\log\dot{\varepsilon}} = \frac{2(2.303)R}{V^*} = 0.042, \tag{9}$$

giving $V^*/N_A = 1.51$ nm^3, the same for dry and wet PLA. Given the PLA density $\rho = 1.24$ g cm^{-3} and the molar mass of lactic acid, $M_0 = 90.078$ g mol^{-1}, the molar volume of lactic acid is estimated as $V_0 = M_0/\rho = 76.6$ cm^3 mol^{-1}, giving a volume per lactic acid unit of 0.128 nm^3. Thus, the activation volume V^* is equivalent to approximately 12 lactic acid units. The fact that the activation volume is the same in dry and wet PLA is explained by the very small water content, amounting to 1–2 water molecules per PLA monomer [25].

To gain further insight into the effect of water in reducing the yield stress, we have conducted additional compression tests on dry samples at 42 °C, so that the ratio T/T_g of the dry PLA is the same as the corresponding ratio for the wet polymer at 37 °C. Stress–strain curves at three strain rates are shown in Fig. S10, and the dependence of the yield stress on the strain rate is shown in Fig. 17. The yield stress of dry PLA at $T = 42$ °C almost coincides with that of wet PLA at $T = 37$ °C (note that the ratio of the testing temperatures in Kelvin is almost equal to unity). The effect of water is thus analogous to an increase in temperature consistent with the temperature increase identified from DMA in Section 4.2, suggesting that the molecular processes mediating viscoelastic deformation and shear plasticity are similar.

Finally, we identified the activation enthalpy from the vertical shift between the σ_y/T curves for dry samples at two different temperatures as:

$$\left(\frac{\sigma_y}{T}\right)_{T=310\text{ K}} - \left(\frac{\sigma_y}{T}\right)_{T=315\text{ K}} = \frac{2}{V^*}\left(\frac{\Delta H}{310} - \frac{\Delta H}{315}\right), \tag{10}$$

giving $\Delta H = 240$ kJ mol^{-1}. Our calculated values for V^* and ΔH are consistent with literature data reported in Section S5.

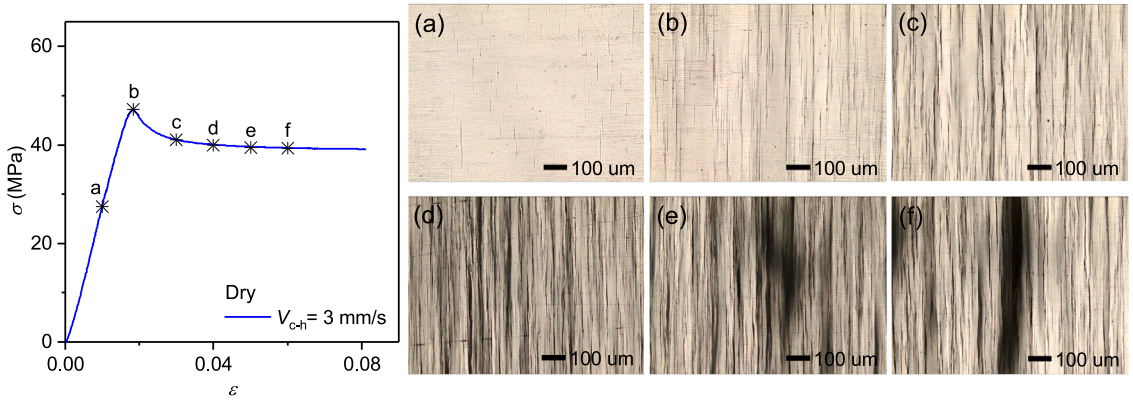

Fig. 13. Transmission optical micrograph of crazing growth in the centre region of gauge length, during tensile deformation of dry PLA. Tension is applied in the horizontal direction.

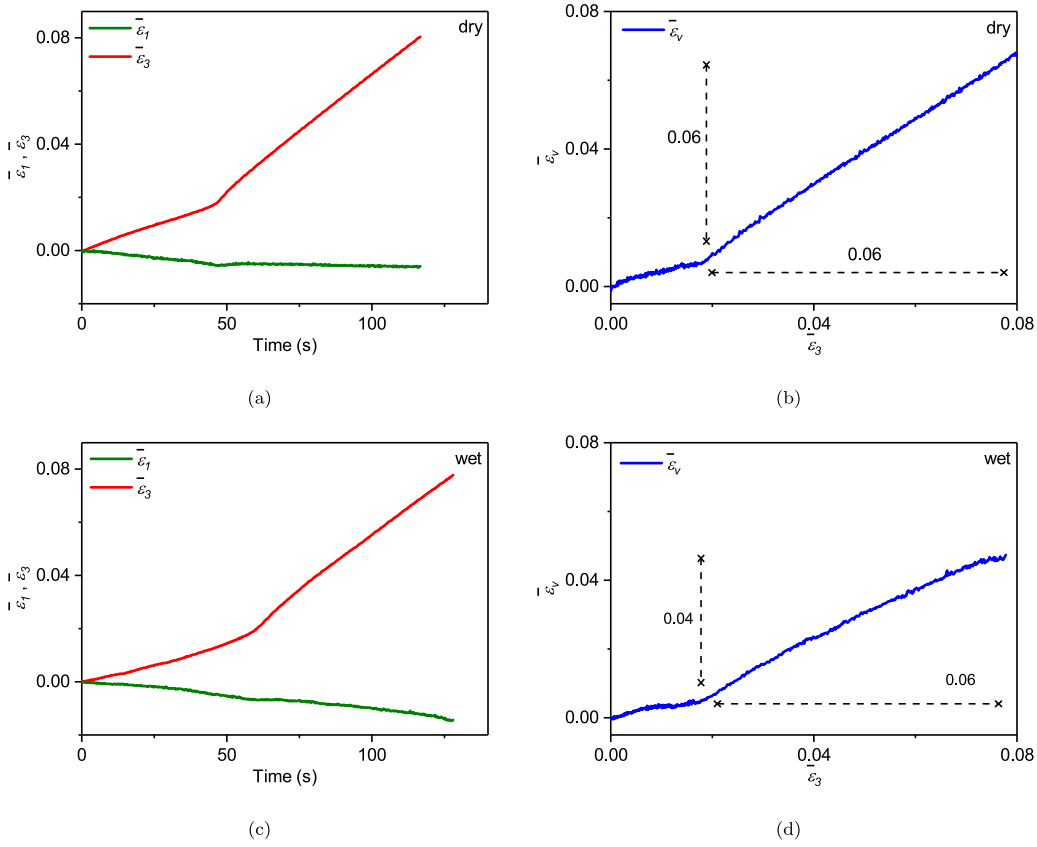

Fig. 14. (a),(c): Total longitudinal and transverse true strains as a function of time in dry and wet specimens loaded at a constant cross-head velocity of 0.03 mm s^{-1}. (b),(d): Corresponding true volumetric strain in dry and wet specimens.

6.2. Tension behaviour

Our experimental results (Section 5.2) suggest that the plastic response of PLA in tension is dominated by craze yielding, rather than shear plasticity. The stress drop is then associated with the spreading of intense crazing across the whole specimen [59]. While craze yielding is the manifestation of underlying damage and can be qualified as brittle-like, the elongation at failure can nevertheless be significant, at least at a slow deformation rate (about 8% strain at a 0.03 mm s^{-1} cross-head velocity). The rate-dependency of the apparent yield stress in craze yielding is also well described by Eyring's Eq. (8). From the slope of the linear regressions in Fig. 11, we calculated an activation volume of $V^*/N_A = 2.54$ nm^3, which corresponds to the volume of approximately 20 lactic acid monomers and is the same for dry and wet PLA. The activation volume in tension has the same order of magnitude than that in compression, but is slightly larger. Compared to shear plasticity, fewer studies have used Eyring's equation to describe the rate dependency of craze yielding [60–62], and the precise physical meaning of the activation volume remains elusive. Here we hypothesise that the activation volume in tension is characteristic of the volume of the molecular segments involved in the drawing of new fibrils from the entangled chain network [63–65]. The thermally-activated character of craze-yielding also explains the rate dependency of the fracture strain (Fig. 12). As the applied deformation rate increases, local molecular rearrangements responsible for craze initiation and widening have less time to take place, leading to higher stress build-up across the network

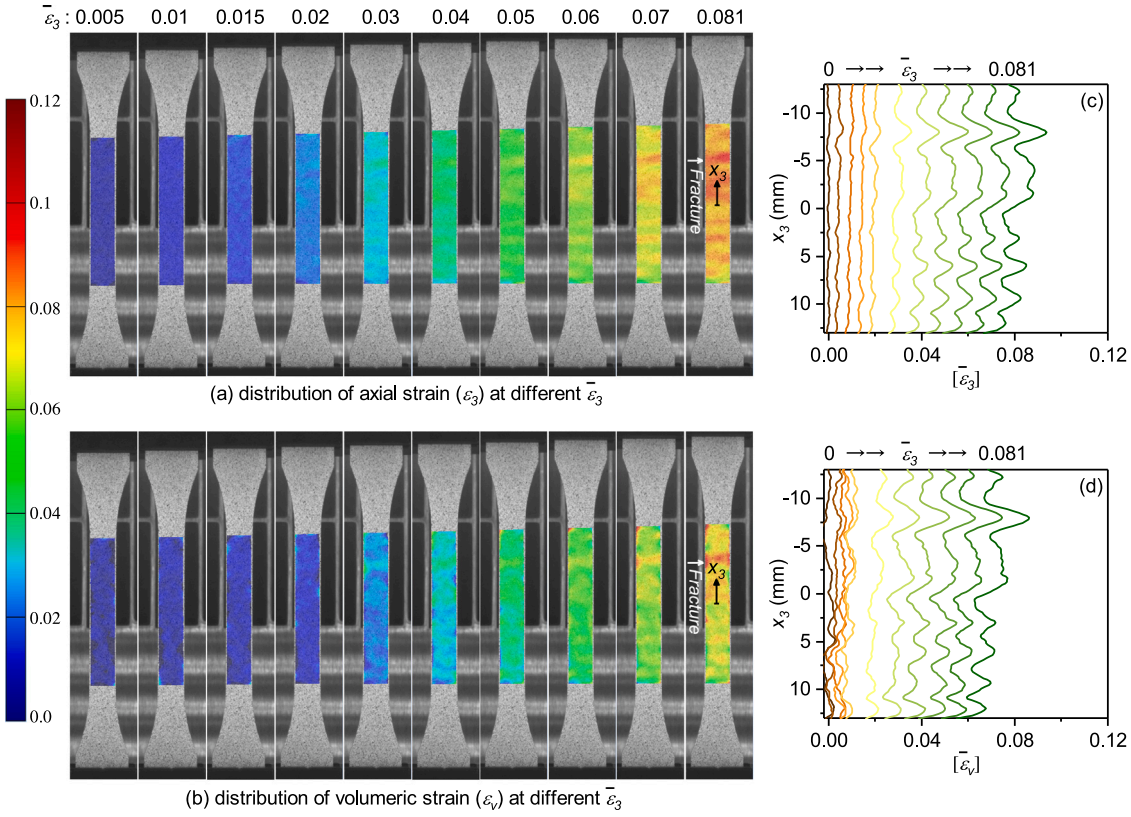

Fig. 15. Fields of (a) ε_3 and (b) ε_v during tensile loading of a dry specimen at a constant cross-head velocity of 0.03 mm/s measured by DIC. The strain $\bar{\varepsilon}_3 = 0.02$ approximately corresponds to the yield strain. (c),(d): Profiles of width-averaged longitudinal strain $[\bar{\varepsilon}_3]$ and volumetric strain $[\bar{\varepsilon}_v]$. Each curve corresponds to a different total strain $\bar{\varepsilon}_3$.

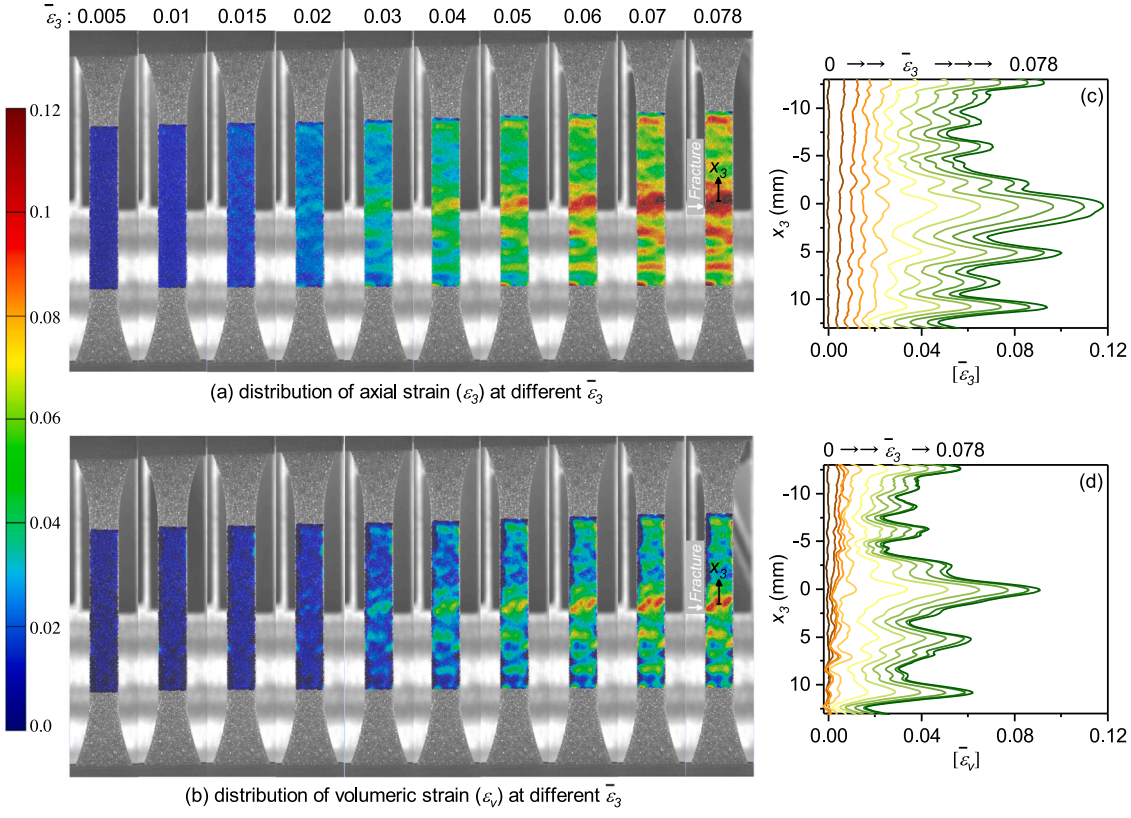

Fig. 16. Fields of (a) ε_3 and (b) ε_v during tensile loading of a wet specimen at a constant cross-head velocity of 0.03 mm/s measured by DIC. The strain $\bar{\varepsilon}_3 = 0.02$ approximately corresponds to the yield strain. (c),(d): Profiles of width-averaged longitudinal strain $[\bar{\varepsilon}_3]$ and volumetric strain $[\bar{\varepsilon}_v]$. Each curve corresponds to a different total strain $\bar{\varepsilon}_3$.

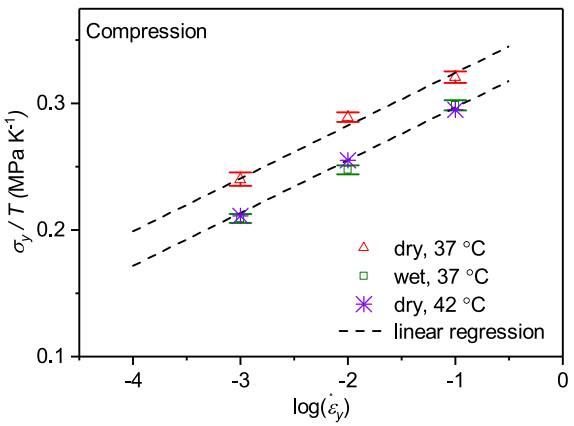

Fig. 17. Strain-rate dependence of the yield stress of dry PLA at two different temperatures (37 °C and 42 °C), compared to that of wet PLA at 42 °C.

and to global brittle failure before significant crazing can take place, as discussed in Ref. [65].

Compared to shear plasticity in compression, the post-yield softening under tension is considerably less pronounced, which may be explained in the following way. In craze yielding, softening has been attributed to craze widening by drawing new polymers into the fibrils, involving intense viscoplastic deformation in the drawing process zone near the craze [66]. In contrast, shear plasticity-induced softening has been attributed to the interaction of shear transformation zones, leading to the development of microscopic shear bands spanning the whole specimen and thickening during deformation [67,68]. In contrast to the local processes involved during crazing, shear plasticity mobilises the majority of the molecular segments across the whole specimen, leading to more pronounced softening.

The development of craze yielding in tension indicates that the critical stress for craze initiation is lower than the critical stress for shear yielding [65]. Indeed, the ratio of the compression yield stress to the tensile yield stress is about 1.5 in our study, for all considered strain rates and for both dry and wet PLA. McCutcheon et al. [18] calculated a crazing initiation stress of 50 MPa for the same PLA grade at a constant cross-head velocity of 1 mm s^{-1}. This value falls between the measured yield stresses at cross-head velocity of 0.3 and 3 mm s^{-1}, consistent with the hypothesis that crazing initiates before yielding in tension.

The development of craze-yielding has also been investigated based on the entanglement density (ν_E), on the basis that polymers with low entanglement density are more prone to disentanglement crazing [13,18,69]. The entanglement density can be calculated as:

$$\nu_E = \frac{\rho N_A}{M_e}, \tag{11}$$

where $\rho = 1.24$ g cm^{-3} is the PLA density, N_A is Avogadro's number, and M_e is the molecular weight of chains between entanglements. For PLA, $M_e = 8700$ g/mol [70], giving $\nu_E = 8.55 \times 10^{25}$ chains/m^3. This value is intermediate between values for polystyrene (crazing-dominated) and polycarbonate (shear yielding-dominated) reported by Kramer [69], supporting possible concurrent craze-yielding and shear-plasticity during tensile testing. The tension behaviour of PLA reported in the present study is actually similar to craze yielding in polystyrene (PS) [59,60,71], to which PLA has often been compared due to the similarities in their physical properties, including high modulus, high strength and low toughness [72].

Although the macroscopic stress–strain responses of dry and wet PLA in tension are similar (Fig. 10), they do exhibit different craze yielding mechanisms. Wet PLA undergoes a combination of shear plasticity and crazing at large deformation, while the response of dry samples remains crazing-dominated with no evidence of shear plasticity (Fig. 14). We attribute this effect to water plasticisation, which could trigger localised shear banding near craze tips at macroscopic stresses lower than the yield stress in the wet PLA. It is also possible that localised shear bands evolve into shear band crazes, interacting with standard crazes, as proposed by Stoclet et al. [13]. Concurrent crazing and shear plasticity in wet samples is supported by the strain heterogeneity pattern (Fig. 16), which shows (i) some inclinations in the longitudinal strain localisation bands, suggesting shear banding and/or shear band crazes and (ii) the presence of regions experiencing negligible volume change. Despite the likely presence of localised shear banding in wet samples, no necking instability was detected, which can be attributed to the stabilising role of volume expansion in preventing the occurrence of necking [13,73]. It is also possible that the presence of water modifies the craze yielding mechanism itself. For example, it has been proposed that the addition of a plasticiser favours the widening of existing crazes with high fibril extension ratio, rather than the creation of new crazes by drawing new stress fibrils [74]. However, Renouf-Glauser et al. reached the opposite conclusion, i.e. plasticity in dry PLA is dominated by craze growth, while it is dominated by new craze formation in wet PLA [75]. Further investigations using for example SAXS experiments would be required to address these questions.

The craze yielding-dominated behaviour of amorphous PLA reported in the present study is consistent with other reports from the literature [18,65,75]. Craze-yielding has also been reported in semi-crystalline PLA grades and PLA blends [13,76–79]. For example, Stoclet et al. [13] showed using SAXS that crazing was responsible for the brittle response of PLA at room temperature. They also showed that the ductile response of PLA at 35 °C involved a combination of shear banding and crazing, and proposed that the interplay between crazing and shear banding could stabilise plastic deformation during neck propagation. However, the presence of a crystalline phase is also known to alter the plasticity mechanism [79]. For example, in Ref. [75], while the deformation of amorphous PLLA was governed by crazing, semi-crystalline PLLA deformed through crystal-mediated deformation with contributions from both cavitation and fibrillated shear. Likewise, Rezgui et al. [14] reported a significant volume change during the tensile deformation of semi-crystalline PLA at 50 °C, but these authors attributed the volume change to void growth, rather than to crazing. Whether crazing or shear plasticity (or a combination of both) dominates in a specific PLA grade also depends on the processing conditions prior to testing. For example, rapid thermal quenching can make amorphous PLA ductile [65]. Melt-stretching of amorphous PLLA has been used to produce ductile semi-crystalline PLLA via the formation of nanocrystals [80]. Conversely, physical aging [65,79] has been shown to results in a more brittle behaviour.

7. Conclusions

We have investigated the thermo-mechanical behaviour of a commercial grade of amorphous PLA in dry and hydrated conditions at body temperature, before the onset of degradation. Characterisation and modelling of the mechanical behaviour of amorphous PLA during degradation will be considered in a future study, building on our recent work on modelling hydrolytic degradation in amorphous polymers [81].

The glass transition temperature of wet PLA determined by DSC was found to be 4.1 °C lower than that of dry PLA, despite the small water uptake at full saturation after 6 hydration days (0.93 wt%). The plasticising effect of water on viscoelastic properties was characterised using DMA, and the Time Temperature Superposition principle was used to generate master curves for the storage modulus of dry and wet PLA at 37 °C over a broad range of frequencies. The plasticising

effect of water depends on frequency, and vanishes at very small and very high frequencies. The horizontal shift between dry and wet master curves corresponds to a temperature raise of 4.5 °C, consistent with the change in glass transition temperature measured by DSC.

Quasi-static uniaxial tests at various strain rates were used to characterise the viscoplastic response of dry and wet amorphous PLA in compression and tension. The compression response of PLA is typical of shear plasticity in glassy polymers, with rate-dependent yield stress followed by pronounced softening and limited rehardening. The presence of water reduces the compression yield stress by 11% on average. In contrast, the tension response predominantly results from craze yielding, as confirmed by direct observation of intense crazing on the sample surface and the very significant volume change measured by DIC, with a 10% decrease in tensile yield stress on average between dry and wet PLA. In dry PLA, crazing accounts for almost all of the plastic deformation, while in wet PLA, it accounts for about two thirds of the plastic deformation, suggesting concurrent craze-yielding and shear plasticity. Furthermore, local strain fields are significantly inhomogeneous, although no necking was observed, which may be due to the stabilising effect of crazes on shear band localisation. The mechanism shift between shear plasticity and craze yielding between tension and compression, and the coexistence of both in wet PLA, have important consequences on structural integrity, which need to be accounted for in designing PLA load-bearing structures, as well as in the development of predictive constitutive models.

CRediT authorship contribution statement

Huanming Chen: Conceptualization, Methodology, Investigation, Validation, Formal analysis, Writing – original draft. **Zhouzhou Pan:** Conceptualization, Methodology, Formal analysis, Writing – review & editing. **Daohe Yuan:** Investigation. **Gregory S. Sulley:** Investigation, Formal analysis. **Reece N. Oosterbeek:** Conceptualization, Writing – review & editing. **Charlotte K. Williams:** Resources, Funding acquisition, Supervision, Writing – review & editing. **Laurence Brassart:** Conceptualization, Methodology, Formal analysis, Funding acquisition, Supervision, Writing – review & editing.

Declaration of competing interest

The authors declare that they have no known competing financial interests or personal relationships that could have appeared to influence the work reported in this paper.

Data availability

Data will be made available on request.

Acknowledgements

This research was supported by UKRI under Award nr. MR/W006995/1. The authors also acknowledge additional support of EPSRC under Awards EP/V003321/1 and EP/S018603/1, and Research England (iCAST, RED, RE-P-2020-04). We would also like to thank Igor Dyson and Nicholas Hawkins for technical support at Oxford University.

Appendix A. Supplementary data

Supplementary material related to this article can be found online at https://doi.org/10.1016/j.polymer.2023.126477.

References

[1] B. Tyler, D. Gullotti, A. Mangraviti, T. Utsuki, H. Brem, Polylactic acid (PLA) controlled delivery carriers for biomedical applications, Adv. Drug Deliv. Rev. 107 (2016) 163–175.
[2] M. Singhvi, S. Zinjarde, D. Gokhale, Polylactic acid: Synthesis and biomedical applications, J. Appl. Microbiol. 127 (6) (2019) 1612–1626.
[3] C. Li, C. Guo, V. Fitzpatrick, A. Ibrahim, M. Zwierstra, P. Hanna, A. Lechtig, A. N., S. Lin, D. Kaplan, Design of biodegradable, implantable devices towards clinical translation, Nat. Rev. Mater. 5 (1) (2020) 61–81.
[4] F. Ebrahimi, H. Ramezani Dana, Poly lactic acid (PLA) polymers: from properties to biomedical applications, Int. J. Polym. Mater. Polym. Biomater. 71 (15) (2022) 1117–1130.
[5] T. Smit, T. Engels, P. Wuisman, L. Govaert, Time-dependent mechanical strength of 70/30 Poly (L, DL-lactide): shedding light on the premature failure of degradable spinal cages, Spine 33 (1) (2008) 14–18.
[6] M. Deroiné, A. Le Duigou, Y.-M. Corre, P.-Y. Le Gac, P. Davies, G. César, S. Bruzaud, Accelerated ageing of polylactide in aqueous environments: Comparative study between distilled water and seawater, Polym. Degrad. Stab. 108 (2014) 319–329.
[7] P.-J. Wang, F. Nezami, M. Gorji, F. Berti, L. Petrini, T. Wierzbicki, F. Migliavacca, E. Edelman, Effect of working environment and procedural strategies on mechanical performance of bioresorbable vascular scaffolds, Acta Biomater. 82 (2018) 34–43.
[8] A. Moetazedian, A. Gleadall, X. Han, V. Silberschmidt, Effect of environment on mechanical properties of 3D printed polylactide for biomedical applications, J. Mech. Behav. Biomed. Mater. 102 (2020) 103510.
[9] C. Fiuza, K. Polak-Kraśna, L. Antonini, L. Petrini, O. Carroll, W. Ronan, T. Vaughan, An experimental investigation into the physical, thermal and mechanical degradation of a polymeric bioresorbable scaffold, J. Mech. Behav. Biomed. Mater. 125 (2022) 104955.
[10] T. Smit, T. Engels, S. Söntjens, L. Govaert, Time-dependent failure in load-bearing polymers: a potential hazard in structural applications of polylactides, J. Mater. Sci.: Mater. Med. 21 (2010) 871–878.
[11] T. Engels, S. Söntjens, T. Smit, L. Govaert, Time-dependent failure of amorphous polylactides in static loading conditions, J. Mater. Sci.: Mater. Med. 21 (2010) 89–97.
[12] S. Söntjens, T. Engels, T. Smit, L. Govaert, Time-dependent failure of amorphous poly-D,L-lactide: Influence of molecular weight, J. Mech. Behav. Biomed. Mater. 13 (2012) 69–77.
[13] G. Stoclet, J.-M. Lefebvre, R. Séguéla, C. Vanmansart, In-situ SAXS study of the plastic deformation behavior of polylactide upon cold-drawing, Polymer 55 (7) (2014) 1817–1828.
[14] F. Rezgui, M. Swistek, J. Hiver, C. G'sell, T. Sadoun, Deformation and damage upon stretching of degradable polymers (PLA and PCL), Polymer 46 (18) (2005) 7370–7385.
[15] A. Bobel, S. Lohfeld, R. Shirazi, P. McHugh, Experimental mechanical testing of Poly(L-Lactide)(PLLA) to facilitate pre-degradation characteristics for application in cardiovascular stenting, Polym. Test. 54 (2016) 150–158.
[16] M. Dreher, S. Nagaraja, J. Bergstrom, D. Hayman, Development of a flow evolution network model for the stress–strain behavior of poly(L-lactide), J. Biomech. Eng. 139 (9) (2017).
[17] J. Sweeney, P. Spencer, G. Thompson, D. Barker, P. Coates, Constitutive modelling of polylactic acid at large deformation using multiaxial strains, Polymers 13 (17) (2021) 2967.
[18] C. McCutcheon, B. Zhao, K. Jin, F. Bates, C. Ellison, Crazing mechanism and physical aging of poly(lactide) toughened with poly(ethylene oxide)-block-poly(butylene oxide) diblock copolymers, Macromolecules 53 (22) (2020) 10163–10178.
[19] S. Mirkhalaf, M. Fagerström, The mechanical behavior of polylactic acid (PLA) films: fabrication, experiments and modelling, Mech. Time-Depend. Mater. 25 (2) (2021) 119–131.
[20] H. Levine, L. Slade, Water as a plasticizer: physico-chemical aspects of low-moisture polymeric systems, Water Sci. Rev. 3 (1988) 79–185.
[21] P. Blasi, S. D'Souza, F. Selmin, P. DeLuca, Plasticizing effect of water on poly (lactide-co-glycolide), J. Control. Release 108 (1) (2005) 1–9.
[22] G. Ozkoc, S. Kemaloglu, Morphology, biodegradability, mechanical, and thermal properties of nanocomposite films based on PLA and plasticized PLA, J. Appl. Polym. Sci. 114 (4) (2009) 2481–2487.
[23] Y. Wang, Y. Qin, Y. Zhang, M. Yuan, H. Li, M. Yuan, Effects of N-octyl lactate as plasticizer on the thermal and functional properties of extruded PLA-based films, Int. J. Biol. Macromol. 67 (2014) 58–63.
[24] D. Li, Y. Jiang, S. Lv, X. Liu, J. Gu, Q. Chen, Y. Zhang, Preparation of plasticized poly (lactic acid) and its influence on the properties of composite materials, PLoS One 13 (3) (2018) e0193520.
[25] O. Vyavahare, D. Ng, S. Hsu, Analysis of structural rearrangements of poly(lactic acid) in the presence of water, J. Phys. Chem. B 118 (15) (2014) 4185–4193.
[26] N. Passerini, D. Craig, An investigation into the effects of residual water on the glass transition temperature of polylactide microspheres using modulated temperature DSC, J. Control. Release 73 (1) (2001) 111–115.

[27] S.E. Atalay, B. Bezci, B. Özdemir, Y.A. Göksu, A. Ghanbari, A. Jalali, M. Nofar, Thermal and environmentally induced degradation behaviors of amorphous and semicrystalline PLAs through rheological analysis, J. Polym. Environ. 29 (2021) 3412–3426.

[28] N. LLC., 4060D safety data sheet, 2023, Accessed:(21/04/2023).

[29] G. Gorrasi, R. Pantani, Effect of PLA grades and morphologies on hydrolytic degradation at composting temperature: Assessment of structural modification and kinetic parameters, Polym. Degrad. Stab. 98 (5) (2013) 1006–1014.

[30] C. Macías, O. Meza, E. Pérez, Relaxation of residual stresses in plastic cover lenses with applications in the injection molding process, Eng. Fail. Anal. 57 (2015) 490–498.

[31] G. Salmoria, L. Vieira, I. Gindri, C. Roesler, E. Fancello, Properties of injection-molded poly (L-co-D,L-lactic acid) using different melt temperatures and stress concentrator in the specimen geometry, Int. J. Adv. Manuf. Technol. 98 (2018) 2231–2237.

[32] T. Tábi, T. Ageyeva, J. Kovács, Improving the ductility and heat deflection temperature of injection molded Poly (lactic acid) products: A comprehensive review, Polym. Test. 101 (2021) 107282.

[33] L. Meinig, R. Boldt, Y. Spoerer, I. Kuehnert, M. Stommel, Correlation between processing parameters, morphology, and properties of injection-molded polylactid acid (PLA) specimens at different length scales, Polymers 15 (3) (2023) 721.

[34] G. Stoclet, R. Séguéla, J.-M. Lefebvre, S. Li, M. Vert, Thermal and strain-induced chain ordering in lactic acid stereocopolymers: influence of the composition in stereomers, Macromolecules 44 (12) (2011) 4961–4969.

[35] Y. Chen, L. Zhao, H. Pan, S. Jia, L. Han, L. Dong, Impact of d-isomer content on the microstructure and mechanical properties of uniaxially pre-stretched poly (lactic acid), Polymer 186 (2020) 122022.

[36] M. Giełdowska, M. Puchalski, S. Sztajnowski, Krucińska, Evolution of the molecular and supramolecular structures of PLA during the thermally supported hydrolytic degradation of wet spinning fibers, Macromolecules 55 (22) (2022) 10100–10112.

[37] MatchID, 2023, Accessed: 2023-03-01, https://www.matchid.eu/.

[38] J. Crank, The Mathematics of Diffusion, Oxford University Press, 1979.

[39] S. Lyu, J. Schley, B. Loy, D. L., C. Hobot, R. Sparer, D. Untereker, Kinetics and time-temperature equivalence of polymer degradation, Biomacromolecules 8 (7) (2007) 2301–2310.

[40] A. Porfyris, S. Vasilakos, C. Zotiadis, C. Papaspyrides, K. Moser, L. Van der Schueren, G. Buyle, S. Pavlidou, S. Vouyiouka, Accelerated ageing and hydrolytic stabilization of poly(lactic acid) (PLA) under humidity and temperature conditioning, Polym. Test. 68 (2018) 315–332.

[41] T. Hatakeyama, K. Nakamura, H. Hatakeyama, Determination of bound water content in polymers by DTA, DSC and TG, Thermochim. Acta 123 (1988) 153–161.

[42] T. Hatakeyama, K. Nakamura, H. Hatakeyama, Vaporization of bound water associated with cellulose fibres, Thermochim. Acta 352 (2000) 233–239.

[43] G. Reich, Use of DSC to study the degradation behavior of PLA and PLGA microparticles, Drug Dev. Ind. Pharm. 23 (12) (1997) 1177–1189.

[44] E.M. Davis, Y.A. Elabd, Water clustering in glassy polymers, J. Phys. Chem. B 117 (36) (2013) 10629–10640.

[45] M.L. Williams, R.F. Landel, J.D. Ferry, The temperature dependence of relaxation mechanisms in amorphous polymers and other glass-forming liquids, J. Am. Chem. Soc. 77 (14) (1955) 3701–3707.

[46] H.F. Brinson, L.C. Brinson, Polymer Engineering Science and Viscoelasticity, Springer, 2008.

[47] A.S. Argon, The Physics of Deformation and Fracture of Polymers, Cambridge University Press, 2013.

[48] S.-M. Zhou, K. Tashiro, T. Ii, Confirmation of universality of time–humidity superposition principle for various water-absorbable polymers through dynamic viscoelastic measurements under controlled conditions of relative humidity and temperature, J. Polym. Sci. B: Polym. Phys. 39 (14) (2001) 1638–1650.

[49] A. Ishisaka, M. Kawagoe, Examination of the time-water content superposition on the dynamic viscoelasticity of moistened polyamide 6 and epoxy, J. Appl. Polym. Sci. 93 (2) (2004) 560–567.

[50] V. Fabre, G. Quandalle, N. Billon, S. Cantournet, Time-temperature-water content equivalence on dynamic mechanical response of polyamide 6,6, Polymer 137 (2018) 22–29.

[51] P.C. Suarez-Martinez, P. Batys, M. Sammalkorpi, J.L. Lutkenhaus, Time–temperature and time–water superposition principles applied to poly (allylamine)/poly (acrylic acid) complexes, Macromolecules 52 (8) (2019) 3066–3074.

[52] A.E. Krauklis, A.G. Akulichev, A.I. Gagani, A.T. Echtermeyer, Time-temperature-plasticization superposition principle: predicting creep of a plasticized epoxy, Polymers 11 (11) (2019) 1848.

[53] C. Siviour, J. Jordan, High strain rate mechanics of polymers: a review, J. Dyn. Behav. Mater. 2 (2016) 15–32.

[54] E. Arruda, M. Boyce, R. Jayachandran, Effects of strain rate, temperature and thermomechanical coupling on the finite strain deformation of glassy polymers, Mech. Mater. 19 (2–3) (1995) 193–212.

[55] M. Barkhad, B. Abu-Jdayil, A.H. Mourad, M. Iqbal, Thermal insulation and mechanical properties of polylactic acid (PLA) at different processing conditions, Polymers 12 (9) (2020) 2091.

[56] A.R. Trivedi, P. Song, C.R. Siviour, Experimentally simulating adiabatic behaviour: Capturing the high strain rate compressive response of polymers using low strain rate experiments with programmed temperature profiles, Polym. Test. 116 (2022) 107773.

[57] L. Van Breemen, T. Engels, E. Klompen, D. Senden, L. Govaert, Rate-and temperature-dependent strain softening in solid polymers, J. Polym. Sci. B: Polym. Phys. 50 (24) (2012) 1757–1771.

[58] G. Ghazaryan, R. Schaller, K. Feldman, T. Tervoort, Rejuvenation of PLLA: Effect of plastic deformation and orientation on physical ageing in poly (L-lactic acid) films, J. Polym. Sci. B: Polym. Phys. 54 (21) (2016) 2233–2244.

[59] J. Hoare, D. Hull, Craze yielding and stress-strain characteristics of crazes in polystyrene, Phil. Mag. 26 (2) (1972) 443–455.

[60] I. Narisawa, Crazing of glassy polymers in alcohols and hydrocarbons, J. Polym. Sci. A-2: Polym. Phys. 10 (9) (1972) 1789–1797.

[61] S. Sjoerdsma, M. Dekkers, D. Heikens, The effect of varying the polyethylene content and the co-polymer content on crazing in polystyrene—low-density polyethylene blends, J. Mater. Sci. 17 (1982) 2605–2612.

[62] M. Dekkers, D. Heikens, Crazing and shear deformation in glass bead-filled glassy polymers, J. Mater. Sci. 20 (1985) 3873–3880.

[63] E. Kramer, L. Berger, Fundamental processes of craze growth and fracture, in: Crazing in Polymers Vol. 2, Springer, 2005, pp. 1–68.

[64] R. Deblieck, D. Van Beek, K. Remerie, I. Ward, Failure mechanisms in polyolefines: The role of crazing, shear yielding and the entanglement network, Polymer 52 (14) (2011) 2979–2990.

[65] M. Razavi, S. Cheng, D. Huang, S. Zhang, S.-Q. Wang, Crazing and yielding in glassy polymers of high molecular weight, Polymer 197 (2020) 122445.

[66] R. Estevez, M. Tijssens, E. Van der Giessen, Modeling of the competition between shear yielding and crazing in glassy polymers, J. Mech. Phys. Solids 48 (12) (2000) 2585–2617.

[67] J. Chevalier, L. Brassart, F. Lani, C. Bailly, T. Pardoen, X. Morelle, Unveiling the nanoscale heterogeneity controlled deformation of thermosets, J. Mech. Phys. Solids 121 (2018) 432–446.

[68] F. Van Loock, L. Brassart, T. Pardoen, Implementation and calibration of a mesoscale model for amorphous plasticity based on shear transformation dynamics, Int. J. Plast. 145 (2021) 103079.

[69] E.J. Kramer, Craze fibril formation and breakdown, Polym. Eng. Sci. 24 (10) (1984) 761–769.

[70] J. Dorgan, J.S. Williams, D. Lewis, Melt rheology of poly (lactic acid): Entanglement and chain architecture effects, J. Rheol. 43 (5) (1999) 1141–1155.

[71] K. Matsushige, S. Radcliffe, E. Baer, The pressure and temperature effects on brittle-to-ductile transition in PS and PMMA, J. Appl. Polym. Sci. 20 (7) (1976) 1853–1866.

[72] R. Drumright, P. Gruber, D. Henton, Polylactic acid technology, Adv. Mater. 12 (23) (2000) 1841–1846.

[73] C. G'sell, J. Hiver, A. Dahoun, Experimental characterization of deformation damage in solid polymers under tension, and its interrelation with necking, Int. J. Solids Struct. 39 (13–14) (2002) 3857–3872.

[74] H. Brown, N. Njoku, The effect of plasticization on craze microstructure, J. Polym. Sci. B: Polym. Phys. 24 (1) (1986) 11–18.

[75] A.C. Renouf-Glauser, J. Rose, D.F. Farrar, R.E. Cameron, The effect of crystallinity on the deformation mechanism and bulk mechanical properties of PLLA, Biomaterials 26 (29) (2005) 5771–5782.

[76] Z. Kulinski, E. Piorkowska, Crystallization, structure and properties of plasticized poly (L-lactide), Polymer 46 (23) (2005) 10290–10300.

[77] H. Liu, N. Chen, S. Fujinami, D. Louzguine-Luzgin, K. Nakajima, T. Nishi, Quantitative nanomechanical investigation on deformation of poly (lactic acid), Macromolecules 45 (21) (2012) 8770–8779.

[78] Z. Bartczak, A. Galeski, M. Kowalczuk, M. Sobota, R. Malinowski, Tough blends of poly (lactide) and amorphous poly ([R, S]-3-hydroxy butyrate) – morphology and properties, Eur. Polym. J. 49 (11) (2013) 3630–3641.

[79] C. McCutcheon, B. Zhao, C. Ellison, F.S. Bates, Crazing and toughness in diblock copolymer-modified semicrystalline poly (L-lactide), Macromolecules 54 (23) (2021) 11154–11169.

[80] M. Razavi, S.-Q. Wang, Why is crystalline poly (lactic acid) brittle at room temperature? Macromolecules 52 (14) (2019) 5429–5441.

[81] Z. Pan, L. Brassart, A reaction-diffusion framework for hydrolytic degradation of amorphous polymers based on a discrete chain scission model, Acta Biomater. 167 (2023) 361–371.